Available online at www.sciencedirect.com

ScienceDirect

Physics Procedia 12 (2011) 666–673

Physics Procedia

LiM 2011

Modeling of phase transformations of Ti6Al4V during laser metal deposition

A. Suárez[a], M. J. Tobar[a], A. Yáñez[a,*], I. Pérez[b], J. Sampedro[b], V. Amigó[c], J. J. Candel[c]

[a]*Universidade da Coruña, Campus de Esteiro s/n, 15403, Ferrol, Spain*
[b]*AIDO/ Nicolás Copérnico, 7-13. Parque Tecnológico, 46980 Paterna, Spain*
[c]*ITM-UPV, c/ Vera s/n, 46022 Valencia*

Abstract

The low density, excellent high temperature mechanical properties and good corrosion resistance of titanium and its alloys have led to a diversified range of successful applications. As a consequence, there is a demand of increasing the capabilities of processing such alloys. The laser cladding technique allows direct metal deposition with an excellent metallurgical bond and a pore free fine grained microstructure. A nonlinear transient thermo-metallurgical model was developed to study the technique with titanium alloys to get a better understanding of the thermal and metallurgical underlying aspects. The calculated temperatures and phase transformations are compared with experimental tests.

Keywords: FEM; simulation; analysis; phase transformations; metallurgical; titanium

1. Introduction

The laser cladding technique [1] allows the deposition of an alloy or coating material on a metal, achieving a good metallurgical bond between both materials, usually a pore free microstructure with fine grains, and thus excellent mechanical properties. Both the adherence of the coating and the tribological behavior are superior to the ones obtained by other techniques such as Atmospheric Plasma Spraying (APS) or High Velocity Oxy-Fuel (HVOF) [2]. In addition, there is a low thermal load transferred to the substrate, generating a smaller heat affected zone (HAZ) and lower distortions in the piece.

The low density, excellent high temperature mechanical properties and good corrosion resistance of titanium alloys have led to a diversified range of successful applications for the demanding performance and reliability requirements of the aerospace, naval, medical, petrochemical, nuclear and power generation industries [3]. Titanium alloys can be used as replacements for aluminum-based materials when the operation temperature exceeds 130ºC, the limit for the aluminum in engineering applications [4]. The aerospace sector makes extensive use of titanium alloys, consuming nearly 70% of the global production, mainly for aeroengine components such as casings, compressor blades and rotors, but also in nacelles and structural parts of the planes [5]. Half of the titanium used is in the form of the alloy Ti6Al4V. Alternatively, as titanium shows very low corrosion rates in human body fluids as

* Corresponding author. Tel.: +34 981337400; Fax: +34 981337410.
E-mail address: ayanez@udc.es

1875-3892 © 2011 Published by Elsevier Ltd.
doi:10.1016/j.phpro.2011.03.083

demonstrated [6], there are applications relevant to the medical industry like prosthetic devices such as artificial heart pumps, heart valve parts as well as load bearing bone such as for hip bone replacement.

2D and 3D FEM models were chosen by many researches to calculate the steady state and transient temperature distributions, and study the influence of several parameters like dilution, powder preheating and its influence in clad height and shape [7-12] Some of these models calculate the stresses or phase transformations based on previous temperature distributions. They studied cracking and base material deflection [13] and the effect of preheating temperature and other laser parameters [14]. There are also models that perform calculations of stress in single and multiple track laser cladding [15-17].

Several authors coupled phase transformation models to their thermal or thermomechanical models in order to simulate laser cladding on carbon steels [18]. In other works [19] a complete phase transformation model based on kinetic data and semiempirical relations, including also the tempering of the martensite is presented. They studied the heat accumulation during part build up due to short idle times or small substrates, calculating the phase distributions and hardness profiles for several cases. There are also 3D thermokinetic models for the laser powder deposition of titanium alloys. They modelled straight [20] tracks as well as L-shaped tracks with sharp and smooth corners.

The authors [15] of this work have developed 3D models for ANSYS, modeling the clad tracks with curved geometries and studying the effect of several parameters on the maximum stresses and maximum bending angles of the cladded plates due to the residual stresses models for ANSYS. They calculated temperatures, strains and stresses for one single track with and without preheating, and also for several clad beads, modeling the clad bead geometry from experimental observation, both for single tracks and for several overlapped tracks.

2. FEM thermal models for laser cladding

A nonlinear transient thermal model was developed for the simulation of the laser cladding process, under the software ANSYS™ [17]. The temperature field inside the materials and its evolution during all the process is computed with a transient thermal analysis. The procedure for the modeling of the clad deposition process, consists in the division of the whole clad track into slices (Figure 1). Then, using the Birth & Death feature, all the elements of the clad track were “killed”, which is a numerical technique that multiplies the heat capacity matrix of these elements by a very small value, usually 10^{-6}, so they virtually disappear from the simulation. During the analysis the elements of each slice are activated at the corresponding load step with its nodes constrained at a temperature above the melting point of the material. Using the conservation of energy, the remaining laser power is applied to the surface of the plate as a heat flux boundary condition with a top hat laser profile centered at the position of the slice being activated. This power is previously weighted by the absorption coefficient of the surface, which also varies with its temperature presenting a step at the melting point of the material. In the samples with several overlapped clad tracks the laser power is partially applied on the surface of the previous clad track. Energy losses by radiation are neglected due to their low relevance and high nonlinearity. Convection with ambient air on all the external active surfaces of the models, including the clad tracks, is considered for the cooling of the samples with a convection coefficient of 40 W/m^2K. The initial temperature of all the nodes was set to the preheating temperature of the samples, which is 549ºC.

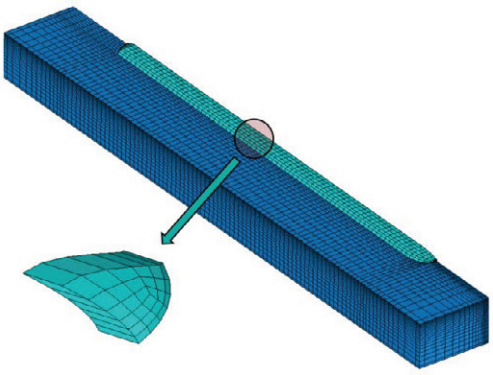

Figure 1. FEM model for one of the tests with one clad track, showing a detail of one of the slices

Models with single clad tracks were created for this study. The meshes have a high density of elements in the zones with higher gradients, with an element size that ranges between 0.1-2 mm. The models are entirely meshed with linear hexahedral elements (Figure 1), which are more accurate and computationally faster. All the models have 20721 elements and 24010 nodes.

The material properties of Ti and Ti6Al4V used in the simulations were obtained from [21] and are represented in Figure 2. The enthalpy formulation was selected instead of the heat capacity, in order to simulate accurately the melting and reduce the convergence problems.

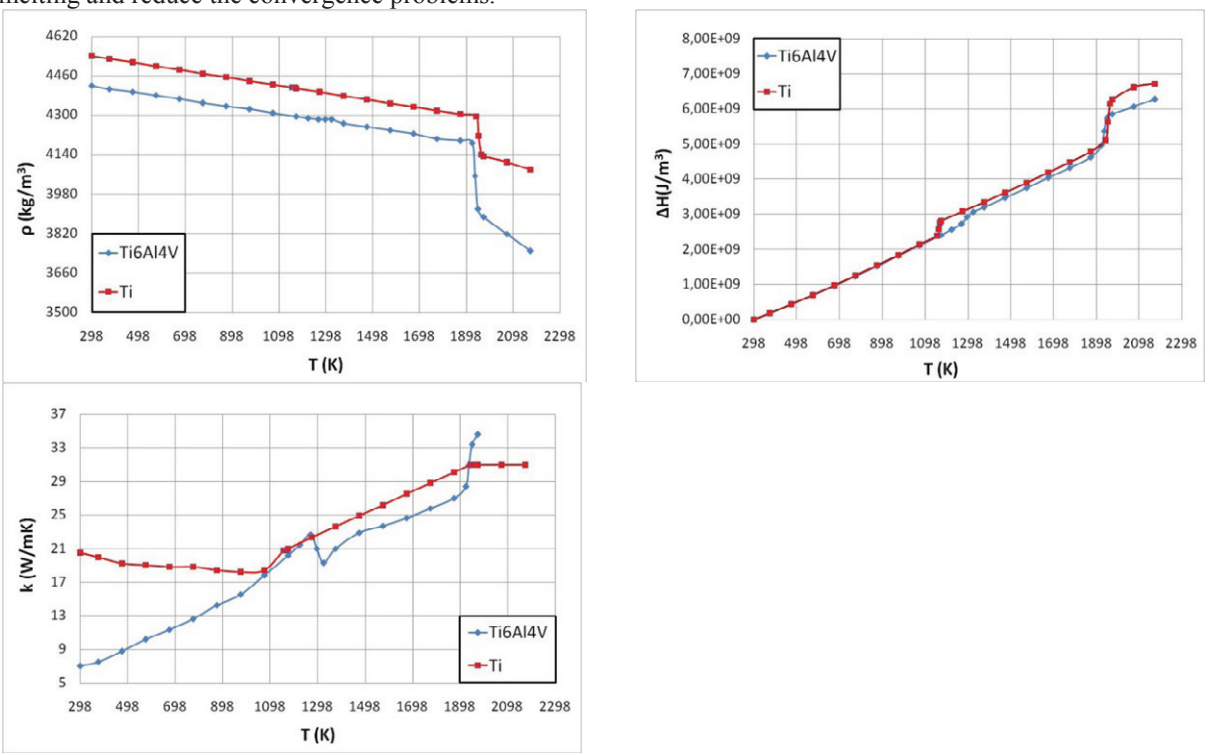

Figure 2. Thermophysical properties of Ti and Ti6Al4V: (a) density; (b) enthalpy; (c) conductivity

3. Model for the phase transformations of Ti6Al4V and Ti

The model for the phase transformations is implemented as a subroutine in ANSYS, and it is fully coupled with the thermal analysis, allowing the calculation of the phase transformations during the ongoing transient simulation. Each load step is solved using a staggered solution procedure commenced by a pure thermal analysis and the subsequent metallurgical analysis. It is not a postprocessing code as other phase transformation models, and therefore allows the change of material properties during the analysis, a feature that is not used in the present study but will be used in future thermomechanical simulations.

The model follows a similar methodology as previous models implemented for metal deposition using TIG welding [22, 23]. It consists of a main subroutine that controls the transition between the different regions of stability of the different phases, according to the temperature range of each region and the element temperature. In some of these regions specific subroutines containing the kinetic models are called from the main subroutine for computing the phase evolution.

The history of several phase changes is calculated and recorded during the whole transient analysis. In order to do that each of the elements of the model has assigned a vector in which all the required information is stored (Figure 3), like temperatures, residence times within the current phase region, phase percentages, auxiliary variables for the kinetic models and a variable that defines the current state of the element. All these vectors are stored in a matrix in which each row corresponds to one element of the model. All of the subroutines are fully vectorized, and therefore the whole phase transformation model is computed very fast.

3.1. Phase transfomations in Ti and Ti6Al4V

The phases considered in Ti6Al4V are α, β, martensite α' and the melted material. The base microstructure of the Ti6Al4V is bimodal, composed mainly by α grains with a low amount of β. During the heating, above the *beta transus* temperature, α phases destabilize and start their transformation to β phase according to the phase diagram. The melted material is also deposited in fully β state. During the cooling down, below the *beta transus* the β phase starts to slowly decompose in α phase. Two different alpha phases are usually distinguished: Widmanstätten and grain boundary [24], although in this study they were considered the same phase, for simplicity considerations. However, if the temperature goes below the martensite start temperature, and the cooling rate is sufficiently high, martensite is formed from the previous β phase. Due to permanence at high temperatures the previously formed martensite can be tempered, decomposing to α or α+β.

Pure titanium presents the transition to β phase and it is even reported to form a quasi-equilibrium martensite with high dislocation density [25]. Therefore the same transformations than in Ti6Al4V were assumed, and due to the lack of experimental kinetic parameters, the same used for Ti6Al4V were used.

3.2. Diffusional phase transformations

The diffusional phase transformations consist of three phases: nucleation, growth and saturation. They are usually assumed to follow the well known Johnson-Mehl-Avrami equation (1) with specific parameters n and k for different transformations and materials:

$$f = 1 - \exp(-kt^n) \tag{1}$$

Where f is the volume fraction of the new phase, t is the isothermal time duration, k is a coefficient dependent on the temperature, composition of parent phase, and grain size, and n is also a coefficient dependent on the type of phase transformation and grain growth. The equation was initially developed for isothermal processes, however it can be applied to non-isothermal processes considering them as composed of a series of isothermal steps [26], and calculating the fictitious time (2) and fictitious volume fraction transformed (3) during these isothermal steps:

$$t_i^* = \left(\frac{-Ln(1 - f_{i-1})}{b_i}\right)^{1/n_i} \tag{2}$$

$$f_i^* = 1 - \exp(b_i(t_i^* + \Delta t)^{n_i}) \tag{3}$$

The volume fraction transformed is obtained by multiplying the fictitious fraction transformed by the maximum volume fraction that can be transformed:

$$f_i = f_i^* f_{max} \tag{4}$$

The temperature dependence is included in the coefficients $b=b(t)$ and $n=n(t)$.

Two diffusional phase transformations were included in the model: the decomposition of $\beta \rightarrow \alpha$, and the tempering of the martensite: $\alpha' \rightarrow \alpha$. The parameters used for the first transformation were obtained from Sha and Malinov [24] and are included in Table 1.

The tempering of the martensite is assumed to transform the existent α' into α according the kinetic parameters obtained from Gil Mur et al. [27], which are also included in Table 1.

3.3. Diffusionless phase transformations

The diffusionless phase transformations considered are the transformation from α and α' to β, which are assumed to transform instantly a volume fraction according to the phase diagram above the *beta transus* temperature, and the

martensitic transformation, which is commonly simulated by the Koinstinen-Marburguer equation (5), with a constant $c=0.003$ for titanium alloys [28]:

$$f_{\alpha'} = 1 - \exp\left(-c(M_s - T)\right) \tag{5}$$

Table 1. Parameters for the JMA equation during the transformations: $\beta \rightarrow \alpha$ and $\alpha' \rightarrow \alpha$

β → α			α' → α		
T (K)	*K*	*n*	*T (K)*	*n*	*k*
1023	*0.0280*	*1.4*	*673*	*0.667*	*0.0192*
1073	*0.0260*	*1.34*	*773*	*1.106*	*0.0147*
1023	*0.0220*	*1.38*	*873*	*1.252*	*0.0246*
1143	*0.0250*	*1.34*	*973*	*1.326*	*0.0307*
1173	*0.0460*	*1.21*			
1193	*0.0240*	*1.39*			
1223	*0.0170*	*1.41*			

4. Experimental

The experimentally obtained specimens were processed with a Nd:YAG laser working in continuous wave, with a top hat profile and a beam diameter on the workpiece of 2 mm. The beam power varies in the interval between 600 and 900 W, and the process velocity shifts between 8 and 12 mm/s. The shielding gas was helium, and the powder feed rate was 2 g/min. The materials used were Ti6Al4V as the material deposited and pure Ti as the substrate. Single and multiple overlapped clad tracks were deposited. The parameters are summarized in Table 2.

Table 2. Parameters of the experimental tests

Test	Power (W)	Velocity (mm/s)
1	700	12
2	600	8
3.	900	12

During the cladding process, temperature measurements were performed using a two color pyrometer, calibrated with furnace tests. The pyrometer was situated perpendicular to the cladding direction, aiming at a fixed point in the plate. The experimental setup is shown in Figure 3.

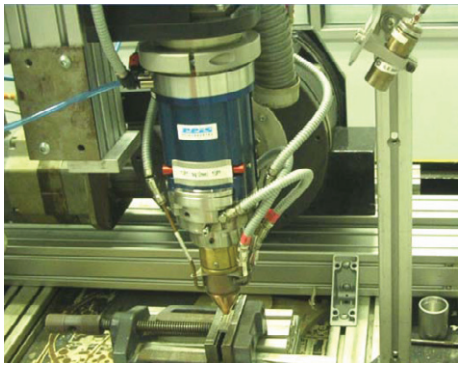

Figure 3. Experimental setup.

All samples were cut transversally, mechanically grounded, polished with silica suspension and etched with Kroll's etch. Cross-sections of the resulting claddings were examined by optical and scanning electron microscopy (SEM). Figure 4 shows the metallographic image of the cross sections of the samples with single clad tracks.

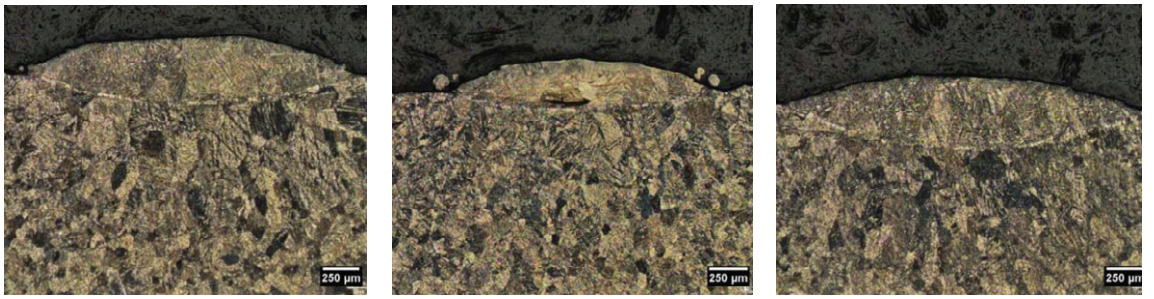

Figure 4. Metallographic picture of the cross sections of the single track samples: (a) 1; (b) 2; (c) 3.

Figure 5a shows the SEM image of the upper part of the clad track in sample 1, with a typical martensitic structure. EDX analyses were carried out in several parts of the clad track to study dilution. In Figure 5b is represented the semi quantitative analysis of the 2 boxes marked in Figure 5a.

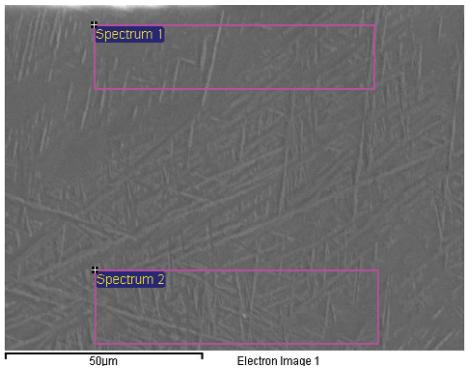

Processing option : All elements analysed (Normalised)

Spectrum	Al	Ti	V	Total
Spectrum 1	5.30	90.87	3.83	100.00
Spectrum 2	5.27	90.74	3.99	100.00
Mean	5.28	90.81	3.91	100.00
Std. deviation	0.02	0.09	0.11	
Max.	5.30	90.87	3.99	
Min.	5.27	90.74	3.83	

All results in weight%

Figure 5. (a) SEM of the upper part of the clad track, test 1; (b) corresponding EDX measurements

5. Results and discussion

The microstructure of the samples was compared with the melted zone and HAZ predicted by the model (Figure 6), obtaining a good agreement in all cases.

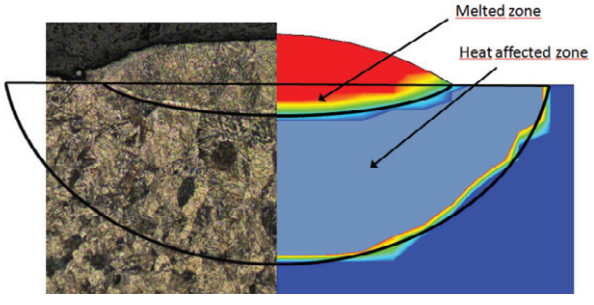

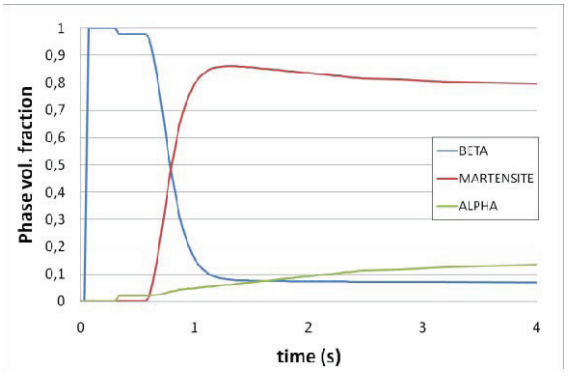

Figure 6. Comparison between the experimentally obtained melted and HAZ and the predicted ones, test 1; (b) phase history of one element of the clad track during the laser cladding of the test 1

The phase history of one element pertaining to the clad track is represented in Figure 6, showing the temporal evolution of all the considered phases. The element is deposited in β phase and starts to transform into martensite below the martensite start temperature. Additionally some β phase transforms into α, as well as a low amount of martensite, which is tempered due to the high residual temperatures at the end of the process. At the end of the simulation, there is a residual fraction of retained β phase untransformed, which was limited to the typical values present in quenched samples.

During the process the pyrometer aimed at a fixed point on the plate, registering a signal which is proportional to the temperature of the measured area. The pyrometer was calibrated with furnace tests; however the measured area had a estimated spot size of about 1.5-2 mm, which is of the approximate same size of the clad tracks. In this area there are points with very different temperatures and emissivity values and therefore the measurements cannot be considered precise. For the comparison with the simulated temperatures, the thermal histories of several nodes were integrated over the area of the pyrometer spot, accounting for the changing geometry and the clad deposition. The comparison is shown in Figure 7, showing an acceptable agreement between both.

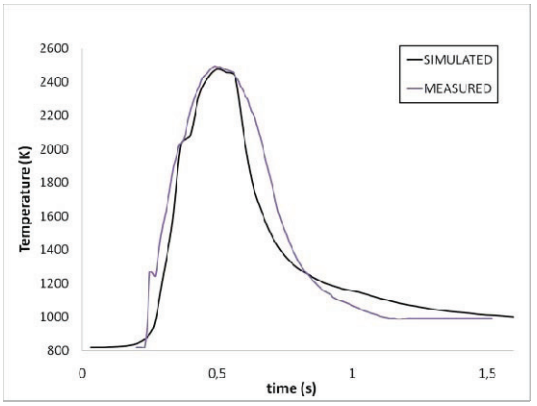

Figure 7. Comparison between the pyrometer measurements and the temperature obtained integrating the simulated thermal histories of several nodes over the spot area of the pyrometer.

6. Conclussions

A transient thermometallurgical model for the simulation of the deposition of Ti6Al4V on pure titanium has been developed. The model consists of several ANSYS subroutines for the simulation of the thermal analysis during the laser cladding technique, plus other subroutines for the implementation of the element-wise phase transformation model in a coupled staggered solution procedure. Diffusional and diffusionless phase transformations during heating, cooling and tempering are simulated by the model.

Experimental tests with single clad tracks were performed. Temperature and phase predictions obtained with the model were compared with microstructural metallographic images, obtaining a good agreement between them. Temperature measurements with the pyrometer were not precise; however there is a reasonable agreement with the simulations.

The present model is intended to be upgraded in subsequent studies using samples with several overlapped and superposed clad tracks, and also to perform mechanical analyses, and study the stress and strain fields during laser metal deposition processes.

Acknowledgements

This work is has been done under the research project MAT2008-06882-C04 funded by the Spanish government (MICIIN).

References

[1] Toyserhani, S. Corbin and A. Khajepour, Laser Cladding (1st ed.), CRC Press (2005).
[2] Khanna, A.S. Kumari, S. Kanungo, S. and Gasser, A. Hard coatings based on thermal spray and laser cladding. In: Int. J. Refract. Met. Hard Mater. 27 (2009), 485-491.
[3] Casalino, G., Curcio, F., Memola, F., Minutolo, C. Investigation on Ti6Al4V laser welding using statistical and Taguchi approaches. In: J. Mater. Process. Technol. 167 (2005), 422–428.
[4] Lima et al. Lima, M.S.F. Laser beam welding of titanium nitride coated titanium using pulse-shaping. In: Mater. Res. 8 (2005), 323–328.
[5] V. N. Moiseyev, Titanium Alloys, Russian Aircraft and Aerospace Applications, Taylor & Francis, 2006.
[6] R. Balasubramaniam, A. Choubey, B. Basu, 2005. Electrochemical behavior of Ti-based alloys in simulated human body fluid environment. Trends Biomater. Artif. Organs
[7] E. Toyserkani, A. Khajepour, S. Corbin, 3-D finite element modeling of laser cladding by powder injection: effects of laser pulse shaping on the process, Optics and Lasers in Engineering,. 41, pp. 849-867, 2004.
[8] J.D. Kim , Y. Peng, Melt pool shape and dilution of laser cladding with wire feeding, Journal of Materials Processing Technology, vol. 104, pp. 284-293, 2000.
[9] J.D. Kim, Y. Peng, Time-dependent FEM simulation of dilution control of laser cladding by adaptative mesh method, KSME International Journal, vol. 14, pp. 177-187, 2000.
[10] G. Zhao, C. Cho, J-D. Kim, Application of 3-D FEM method using Lagrangian formulation to dilution control in laser cladding process, International Journal of Mechanical Sciences, vol. 45, pp. 777-796, 2003.
[11] C. Cho, G. Zhao, S-Y. Kwak, C.B. Kim, Computational mechanics of laser cladding process, Journal of Materials Processing Technology, vol. 153-154, pp. 494-500, 2004.
[12] S. Kumar, S. Roy, Development of theoretical process maps to study the role of powder preheating in laser cladding, Computational Materials Science, vol. 37, pp. 425-433, 2006.
[13] A.H. Nickel, D.M. Barnett, F.B. Prinz, Thermal stresses and deposition patterns in layered manufacturing, Materials Science and Engineering, vol. 317, pp. 59-64, 2001.
[14] A. Vasinonta, J.L. Beuth, M.L. Griffith, Process maps for laser deposition of thin-walled structures, in Proceedings 1999 Solid Freeform Fabrication Symposium, Austin, TX, USA, 1999, pp. 383-391.
[15] M.J. Tobar, A. Suárez-Díaz, J.C. Álvarez, J. M. Amado, A. Yáñez, A 3D transient FEM analysis of residual stress generation during laser cladding.: Proceedings of the LANE 2007, 2007.
[16] H-T. Zhang, C-H. Xu, X-Q. Yang H-Y. Zhao, Termperature and stress fields of multi-track laser cladding, Trans. Nonferrous Met. Soc. China, vol. 19, pp. 495-501, 2009.
[17] A. Suárez, J.M. Amado, M.J. Tobar, A. Yáñez, E. Fraga, M.J Peel, Study of residual stresses generated inside laser cladded plates using FEM and diffraction of synchrotron radiation, Surface and Coatings Technology, vol. 204, pp. 1983-1988, 2010.
[18] F. Brückner, D. Lepski, E. Beyer, FEM calculations of thermally induced stresses in laser cladded coatings. Munich: Proc. LIM, Lasers in Manufacturing, pp. 97-103, 2007.
[19] R. Vilar, T. Reti, A.M. Deus L. Costa, Rapid tooling by powder deposition: Process simulation using finite element analysis, Acta Materialia, vol. 53, pp. 3987-3999, 2005.
[20] A. Crespo, A. Deus, R. Vilar, Finite element analysis of laser poeder depositin of titanium.: ICALEO 2006 Congress Proceedings, Scottsdale, AZ , 2005.
[21] K. C. Mills, Recommended values of thermophisical properties for selected commercial alloys. In: ASM International, Woodhead Publishing Ltd., 2002.
[22] C. Charles, N. Järvstrat, Development of a Microstructure Model for Metal Deposition of Titanium Alloy Ti-6Al-4V. Proceedings of the 11th World Conference on Titanium (Ti-2007), Kyoto, Japan, 2007
[23] C. Charles, N. Järvstrat, Modelling Ti-6Al-4V microstructure by evolution laws implemented as finite element subroutines: Application to TIG metal deposition, Proceedings of the 8 th International Conference on Trends in Welding Research, Pine Mountain, GA, USA, 2008
[24] W. Sha, S. Malinov, Titanium alloys: modelling of the microstructure, properties and applications. CRC Press, 2009.
[25] Y.L. Kao, G.C. Tu, C.A. Huang, T.T. Liu, A study on the hardness variation of α- and β-pure titanium with different grain sizes, Materials Science and Engineering A, 398 (2005), pp. 93-98
[26] C. H. Gür, J.Pan, Handbook of Thermal Process Modeling of Steels. Taylor & Francis, 2009.
[27] F.X. Gil Mur, D. Rodríguez, J.A. Planell, Influence of tempering temperature and time on the Ti-6A1-4V martensite, Journal of Alloys and Compounds, 234 (1996), pp. 287-289.
[28] Y. Fan, P. Cheng, et al., Effect of phase transformations on laser forming of Ti-6Al-4V alloy, Journal of Applied Physics, 98, 013518 (2005).